Direct Measurement and Theoretical Calculation of the Rate Coefficient for Cl + CH₃ in the Range from $T = 202-298$ K

James K. Parker,[†] Walter A. Payne,[‡] Regina J. Cody,* Fred L. Nesbitt, and Louis J. Stief

Solar System Exploration Division, NASA/Goddard Space Flight Center, Greenbelt, Maryland 20771

Stephen J. Klippenstein[§]

Combustion Research Facility, Sandia National Laboratories, Livermore, California 94551-0969

Lawrence B. Harding

Chemistry Division, Argonne National Laboratory, Argonne, Illinois 60439

Received: September 22, 2006

The rate coefficient has been measured under pseudo-first-order conditions for the Cl + CH₃ association reaction at $T = 202$, 250, and 298 K and $P = 0.3-2.0$ Torr helium using the technique of discharge-flow mass spectrometry with low-energy (12-eV) electron-impact ionization and collision-free sampling. Cl and CH₃ were generated rapidly and simultaneously by reaction of F with HCl and CH₄, respectively. Fluorine atoms were produced by microwave discharge in an approximately 1% mixture of F₂ in He. The decay of CH₃ was monitored under pseudo-first-order conditions with the Cl-atom concentration in large excess over the CH₃ concentration ($[Cl]_0/[CH_3]_0 = 9-67$). Small corrections were made for both axial and radial diffusion and minor secondary chemistry. The rate coefficient was found to be in the falloff regime over the range of pressures studied. For example, at $T = 202$ K, the rate coefficient increases from 8.4×10^{-12} at $P = 0.30$ Torr He to 1.8×10^{-11} at $P = 2.00$ Torr He, both in units of cm³ molecule⁻¹ s⁻¹. A combination of ab initio quantum chemistry, variational transition-state theory, and master-equation simulations was employed in developing a theoretical model for the temperature and pressure dependence of the rate coefficient. Reasonable empirical representations of energy transfer and of the effect of spin−orbit interactions yield a temperature- and pressure-dependent rate coefficient that is in excellent agreement with the present experimental results. The high-pressure limiting rate coefficient from the RRKM calculations is $k_2 = 6.0 \times 10^{-11}$ cm³ molecule⁻¹ s⁻¹, independent of temperature in the range from 200 to 300 K.

Introduction

Methane is an important trace species in Earth's atmosphere.[1] In the stratosphere, it reacts with chlorine atoms to produce HCl and methyl radicals[2]

$$Cl + CH_4 \rightarrow HCl + CH_3 \qquad (R1)$$

This is the main process that converts active Cl to the relatively unreactive reservoir species HCl in the stratosphere. It is especially important to have reliable kinetics data for R1, as it is well-established that chlorine atoms catalytically convert ozone to oxygen.[3] Despite extensive theoretical and experimental investigations of R1, values of the rate coefficient at low temperatures are uncertain. In the range of 215−220 K, the rate coefficient for R1 has been measured by various groups,[4−11] and the results differ by as much as a factor of 2. A difference of only 27% in the value of the rate coefficient has been shown to have a substantial effect on the calculated abundance of stratospheric HCl.[12]

A suggestion has been made in the literature that methyl radicals formed in R1 can contribute to the observed loss of Cl

atoms in experimental kinetics studies of R1.[8] Therefore, it is desirable to have reliable kinetics data for the reaction

$$CH_3 + Cl + M \rightarrow CH_3Cl + M \qquad (R2)$$

so that corrections can be made to the bimolecular rate coefficient of R1, if necessary. To date, there have been no direct measurements of the rate coefficient for R2. The only available data are from a very complex system, the photochlorination of methane.[13] The experiments were performed at $P = 50-300$ Torr CO₂ and $T = 298-423$ K and yielded $k_2 = 3.7 \times 10^{-10}$ exp($-185/T$) cm³ molecule⁻¹ s⁻¹, independent of pressure. The amount of uncertainty in this Arrhenius expression for k_2 is very large because of the indirect way in which it was derived.

Because of the large uncertainty in the available kinetics data for R2 and its possible role in perturbing laboratory measurements of k_1, we have undertaken a direct measurement of k_2 in the ranges $T = 202-298$ K and $P = 0.3-2.0$ Torr helium. We use the technique of discharge-flow mass spectrometry with low-energy (12-eV) electron-impact ionization and collision-free sampling to follow the CH₃ signal in an excess concentration of chlorine atoms. Helium was chosen as the bath gas in these experiments because most low-temperature kinetics experiments on R1 have been carried out in helium.

We have also developed a theoretical model for the temperature and pressure dependence of k_2 incorporating a combination

* Corresponding author. E-mail: Regina.J.Cody@nasa.gov.
[†] Current address: Midwest Research Institute, 425 Volker Blvd., Kansas City, MO 64110.
[‡] Deceased.
[§] Current address: Chemistry Division, Argonne National Laboratory, Argonne, IL 60439.

1016 *J. Phys. Chem. A, Vol. 111, No. 6, 2007*

Parker et al.

of multireference configuration-interaction calculations of the interaction potential, variable-reaction-coordinate transition-state-theory calculations of the microcanonical/*J*-resolved rate coefficients, and master-equation simulations of the thermal rate coefficient. Excellent agreement with the present experimental results was obtained with reasonable empirical representations of the energy-transfer process and of the effect of spin−orbit interactions. Unfortunately, ambiguities in the appropriate treatment of spin−orbit effects preclude definitive theoretical estimates for the high-pressure-limit rate coefficient. Nevertheless, the modeling process demonstrates that the present experimental observations are incompatible with the high-pressure limit obtained by Timonen et al.[13] Instead, the present study suggests a high-pressure-limit rate coefficient that is about a factor of 4 lower, i.e., $\sim 6 \times 10^{-11}$ cm^3 molecule^{-1} s^{-1}. Furthermore, these experimental results are consistent with a barrier-free combination of Cl atoms and methyl radicals.

Experimental Section

The discharge-flow mass spectrometry apparatus has been described in previous publications.[14,15] The experiments were performed in a Pyrex flow tube of about 100-cm length and 2.8-cm diameter. The inner surface of the flow tube was lined with Teflon FEP. The flow tube was fitted with a Pyrex movable injector that was positioned between 4 and 44 cm from the sampling pinhole during kinetics experiments. Reactions were studied in He carrier gas with the linear gas velocity (plug flow) in the range of 2400−2700 cm s^{-1}. Flow rates were measured by calibrated MKS flow meters for the following: helium (Air Products, 99.9995%), the F$_2$/helium mixture (1% F$_2$ in He; original mixture from Spectra Gases, 5% mixture of F$_2$ in He, initially 99.0% pure F$_2$ and 99.9995% pure He), the CH$_4$/helium mixture (1.3% CH$_4$, balance helium; CH$_4$ from MG Industries, 99.9995%), HCl (Air Products, 99.997%), and the Cl$_2$/helium mixture (5% Cl$_2$; Air Products, 99.998% pure in Cl$_2$). The Cl$_2$/helium mixture was made by diluting pure Cl$_2$ with helium after a freeze−pump−thaw cycle on pure Cl$_2$.

The concentrations of the gases in the flow tube were calculated from the flow rates and the total pressure as measured with an MKS Baratron manometer. The pressure in the flow tube was controlled by varying the position of a throttling valve; pressures ranged from $P = 0.3-2.0$ Torr. The flow tube was used at ambient temperature or cooled by circulating ethanol from a cooled reservoir through the jacket surrounding the tube. At $T = 202$ K, the temperature profile was flat (± 1 K) from 3 to 44 cm. The flow tube was coupled via a two-stage collision-free sampling system to a quadrupole mass spectrometer (ABB Extrel).

Fluorine atoms were produced by microwave discharge (~ 60 W, 2450 MHz, Opthos Instruments) in a 1% mixture of F$_2$ in He. The discharge region consisted of a $^3/_8$-in. ceramic tube coupled to a glass discharge arm. Fluorine atoms entered the flow tube at $d \approx 80$ cm upstream from the first pinhole.

During kinetics measurements, HCl and CH$_4$ were introduced into the system via the movable injector. The reaction time for R2 was then controlled by moving the injector under the condition of constant linear gas velocity. Chlorine atoms and CH$_3$ radicals were generated rapidly and simultaneously by reactions[16,17]

$$F + HCl \rightarrow Cl + HF \qquad (R3)$$

$$k_3(139-294 \text{ K}) = 6.99 \times 10^{-12} \text{ (cm}^3 \text{ molecule}^{-1} \text{ s}^{-1})$$
$$\exp(-9 \text{ K}/T)$$

$$F + CH_4 \rightarrow CH_3 + HF \qquad (R4)$$

$$k_4(180-410 \text{ K}) = 1.3 \times 10^{-10} \text{ (cm}^3 \text{ molecule}^{-1} \text{ s}^{-1})$$
$$\exp(-215 \text{ K}/T)$$

HCl and CH$_4$ were in large excess over F with the ratio [HCl + CH$_4$]/[F] = 33/1−240/1.

In separate experiments, the concentration of F atoms was determined by measuring the Cl$_2$ consumption in the temperature-independent fast "titration reaction"[18]

$$F + Cl_2 \rightarrow FCl + Cl \qquad (R5)$$

$$k_5(180-360 \text{ K}) = 6.0 \times 10^{-11} \text{ cm}^3 \text{ molecule}^{-1} \text{ s}^{-1}$$

With Cl$_2$ in excess, the fluorine-atom concentration was determined by measuring the decrease in the Cl$_2$ signal ($m/z = 70$) at an electron energy of 16.8 eV when the discharge was initiated. The dilute Cl$_2$/He mixture was admitted via the movable injector. The titration reaction was carried out with the position of the injector ($d = 20$ cm) chosen to ensure that R5 went to completion and that the injector was at approximately the midpoint of the CH$_3$ decay. The absolute fluorine-atom concentration is given by

$$[F]_0 = [Cl_2]_{\text{Disc Off}} - [Cl_2]_{\text{Disc On}} \equiv (\Delta Cl_2 \text{ signal})[Cl_2]_{\text{Disc Off}} \qquad (1)$$

where ΔCl_2 signal is the fractional decrease in the Cl$_2$ signal, $(S_{\text{Disc Off}} - S_{\text{Disc On}})/S_{\text{Disc Off}}$. The concentration range of fluorine atoms in the experiments was $(2.4-17.0) \times 10^{12}$ atoms cm^{-3}. This yielded initial Cl/CH$_3$ concentration ratios ([Cl]$_0$/[CH$_3$]$_0$) of 9−67. Previous experience has shown that, in this flow system, the absolute concentration of F is invariant along the flow tube for injector positions of 2−44 cm[15b] and 10−40 cm[15d].

The initial HCl and CH$_4$ concentrations ([HCl]$_0$ and [CH$_4$]$_0$, respectively) were adjusted to produce the desired initial Cl/CH$_3$ concentration ratios, R, by using the values given above for k_3 and k_4, as shown in the expression

$$R = \frac{[Cl]_0}{[CH_3]_0} = \frac{k_3[HCl]_0}{k_4[CH_4]_0} \qquad (2)$$

The initial concentrations of Cl and CH$_3$ ([Cl]$_0$ and [CH$_3$]$_0$, respectively) were calculated from the measured initial fluorine-atom concentration ([F]$_0$) and the ratio R as given by

$$[Cl]_0 = [F]_0\left(\frac{R}{1+R}\right) \qquad (3)$$

$$[CH_3]_0 = [F]_0 - [Cl]_0 \qquad (4)$$

The range of initial concentrations of HCl in these experiments was $(4.53-6.65) \times 10^{14}$ molecules cm^{-3}, and the range of initial concentrations of CH$_4$ in these experiments was $(0.97-6.04) \times 10^{12}$ molecules cm^{-3}. Formation of Cl and CH$_3$ was complete within about 2 ms. A stochiometry correction of the form

$$[Cl]_{\text{mean}} = [Cl]_0 - [CH_3]_0/2 \qquad (5)$$

was made to the initial chlorine-atom concentration, [Cl]$_0$. The range of initial Cl concentrations in these experiments was $(2.26-16.7) \times 10^{12}$ atoms cm^{-3}, and the range of initial CH$_3$ concentrations in these experiments was $(1.25 - 6.79) \times 10^{11}$ molecules cm^{-3}, with all but two experiments having [CH$_3$]$_0$ < 5×10^{11} molecules cm^{-3}.

As was the case for fluorine atoms, previous experience[15c] has consistently demonstrated, using three different methods to determine the chlorine-atom concentration, that first-order wall losses for atomic chlorine in this flow system are small. This was verified for this study by measuring the first-order wall loss for chlorine atoms in a separate set of experiments at $P = 1$ Torr for $T = 202$ and 298 K. The chlorine atoms were generated by reaction R3 with $[HCl]_0 = 6.3 \times 10^{14}$ molecules cm^{-3} and $[F]_0 \equiv [Cl]_0 = 7.9 \times 10^{12}$ or 2.8×10^{12} atoms cm^{-3}. The chlorine atoms were monitored in a limited *m/z* scan range of 34.5−35.2 amu to considerably limit the overlap from the adjacent HCl$^+$ mass peak. The chlorine-atom signal was measured as the distance from the sampling pinhole to the end of the movable injector both increased (from 5 to 44 cm) and decreased (from 44 to 5 cm). The net signal from the chlorine atoms was obtained by subtraction of the background signal from the total signal. The natural logarithm of the net signal was graphed versus time to yield a pseudo-first-order rate coefficient from the slope. The reaction time was derived from the measured distance between the tip of the movable injector and the pinhole and the linear velocity of the gas, calculated from the measured pressure and gas flow rates. At $T = 202$ K, no loss of chlorine atoms occurred along the flow tube. At $T = 298$ K, the loss of chlorine atoms along the flow tube was negligible, although a small perturbation in the chlorine-atom signal occurred at the position of the side arm to the pressure gauge (approximately 27 cm from the sampling pinhole).

CH$_3$ radicals were detected at *m/z* = 15 following low-energy (∼12-eV) electron-impact ionization to minimize any contribution to the CH$_3$ signal from dissociative ionization of CH$_4$, which was present in large excess over CH$_3$ radicals. The observed CH$_3$ signal was corrected to yield the net signal by subtracting the background signal measured with the microwave discharge off; the background signal includes both the instrument background and a small contribution from the dissociative ionization of CH$_4$.

Theoretical Section

Potential Energy Surface. One set of electronic structure calculations was used to characterize the long-range interaction potential between Cl and CH$_3$, and a second set of electronic structure calculations was used to determine, as accurately as possible, the C−Cl bond energy of CH$_3$Cl. The former was used to determine the high-pressure limit of the CH$_3$ + Cl combination reaction, the latter for modeling of the pressure dependence. In this section, we describe first the calculation of the potential surface and then the calculation of the bond energy.

Electronic structure calculations of the long-range potential surface were carried out for the lowest three singlet surfaces. For large separations between reactants, the singlet wavefunctions are inherently multireference in character. For this reason, we used multireference configuration-interaction (MR−CI) calculations employing orbitals optimized with a state-averaged, complete-active-space, self-consistent-field (CASSCF) methodology.[19,20] In these calculations, the CASSCF reference wavefunctions consisted of four active orbitals and six active electrons. The four active orbitals were the CH$_3$ radical orbital and the three Cl 3p orbitals. All of the calculations were performed in C_s symmetry. In this point group, three of the active orbitals are of A′ symmetry, and one is of A″ symmetry. The orbitals were optimized for an equally weighted average of the 1^{1}A′, 2^{1}A′, and 1^{1}A″ states. The energies of these three individual states were then obtained using multireference, singles and doubles configuration-interaction calculations,[21,22] employ-

ing the same CAS reference space as described above. The effects of higher-order excitations were tested using a multi-reference Davidson correction. The basis set used in all of the potential surface calculations was the correlation-consistent, augmented polarized valence triple-ζ (aug-cc-pvtz) basis set of Dunning.[23,24]

All three of these states correlate with CH$_3$(1^{2}A″) + Cl(1^{2}P) and at long range are degenerate at this level of theory. Only one of these three states is reactive, and so, to fit the reactive surface, we simply chose the lowest of the three states at each geometry. A more accurate treatment, including spin−orbit coupling, which will split the long-range degeneracy of these states, is planned for the future.

In all of the potential surface calculations, the structure of the CH$_3$ radical was kept fixed at its equilibrium geometry. The potential surface calculations were done in a single plane, the plane perpendicular to the plane of the CH$_3$ radical, containing one of the CH bonds of the CH$_3$ radical (CH$_a$) and bisecting the other two CH bonds. Three coordinates were used to specify a point in this two-dimensional plane. These three coordinates are the C−Cl distance, R; the angle between the C−Cl bond and the C_3 axis of CH$_3$, θ; and the dihedral angle between the CH$_a$−C_3 plane and the C−Cl−C_3 plane, ϕ. Using these three coordinates, (R, θ, ϕ), a $26 \times 10 \times 2$ three-dimensional grid of points was calculated, where R varied from 3.5 to 20.0 au in uneven increments, θ varied from 0° to 90° in 10° increments, and ϕ had a value of either 0° or 180°. A three-dimensional analytic potential was then constructed by fitting the (R, θ) grids with two-dimensional splines and assuming a cos(3ϕ) dependence for ϕ, the coefficient of which was determined to fit the difference between the energies of the points (R, θ, 0°) and (R, θ, 180°). This analytic potential is available from the authors upon request. Note that the next nonzero term in the Fourier expansion of the ϕ would be cos(6ϕ). In these calculations, the cos(6ϕ) and higher terms were neglected.

The bond dissociation energy for CH$_3$Cl → CH$_3$ + Cl was determined from spin-restricted QCISD(T)[25] calculations. Results obtained with Dunning's correlation-consistent polarized valence triple- and quadruple-ζ basis sets[26] were extrapolated to the infinite-basis-set limit via the expression[27,28]

$$E(\infty) = E(l_{max}) - B/(l_{max} + 1)^4 \qquad (6)$$

where l_{max} is the maximum angular momentum in the basis set. After zero-point and spin−orbit corrections, a bond dissociation energy of 82.1 kcal/mol was obtained. The geometric structures and zero-point energies employed in this analysis were obtained from density functional theory employing the Becke-3 Lee−Yang−Parr (B3LYP) functional[29] and the 6-311++G(d,p) basis set.[30] Unrestricted wave functions were employed in these B3LYP optimizations and vibrational analyses.

The MOLPRO quantum chemistry software was employed in all quantum chemistry calculations described here,[31] except for the B3LYP evaluations, which employed the Gaussian 98 software.[32]

Kinetics. Microcanonical/*J*-resolved rate coefficients were evaluated from variable-reaction-coordinate transition-state theory[33] employing the above-described CAS+1+2+QC/aug-cc-pvtz analytic potential energy surface. This approach involves the minimization of the transition-state number of states with respect to both the CH$_3$···Cl separation and the location of a pivot point in the CH$_3$ fragment. This pivot point specifies the shape of the transition state dividing surface. Various locations of the pivot point along the C_3 axis were considered, with the optimal location for this system generally being the C atom. The

analogous pivot point for monatomic fragments, such as the Cl atom, is necessarily located at the atom itself.

The strong spin−orbit interaction in the Cl atom presents certain difficulties and ambiguities in the calculation of the microcanonical/*J*-resolved rate coefficients. The present CAS+1+2+QC calculations did not include the spin−orbit effect. For the Cl atom as a reactant, we included the spin−orbit states in the standard fashion, i.e., as a direct sum over the spin−orbit states with their full spin and orbital degeneracies. At large separations, the spin−orbit splittings are largely conserved, and the interaction potential corresponds to the long-range interaction potential plus the spin−orbit splitting. The ground electronic state then has an effective degeneracy of 8 arising from the quartet degeneracy of the $^2P_{3/2}$ state of the Cl atom and the doublet spin degeneracy of the CH_3 radical. At short separations, only the lowest singlet state is strongly attractive.

A proper statistical treatment of the different electronic states requires some knowledge of the strength and variation in the spin−orbit interactions in the transition-state region. Unfortunately, this information is not readily available. Thus, we were forced to resort to certain simplifying assumptions arising from the observation that, in radical−radical reactions, there are generally two fairly well separated transition-state regions. In the inner transition-state region, i.e., at short separations, the spin−orbit splitting is greatly reduced, and we assumed that it could be ignored. Thus, the interaction potential in the inner transition-state region was taken to be that from the CAS+1+2+QC evaluations (which ignored the spin−orbit splitting in defining the interaction) shifted up relative to the ground state of the product by the base spin−orbit shift of 294 cm^{-1}. In the region of the outer transition state, i.e., at large separations, we assumed that the spin−orbit splitting was equivalent to its asymptotic value for the Cl atom. The overall transition-state number of states was then taken to be the minimum of the number at large separations employing an electronic degeneracy of 8 and the number at short separations, where the electronic degeneracy corresponds to unity, but with the interaction potential shifted up by the spin−orbit constant of 294 cm^{-1}. A recent article by Schinke and co-workers on the O + O_2 reaction provides further rationale for some of these assumptions,[34] as does an earlier study of the NCNO dissociation into CN + NO.[35]

The ambiguity in this approach is that it can depend on the separation at which we switch from the long-range assumptions to the short-range assumptions. For our recent study of the reaction of various hydrocarbon radicals with an O atom,[36] this dependence was quite weak and yielded uncertainties on the order of 10%. Here, however, because of the greater spin−orbit splitting in Cl relative to that in O, this dependence is quite strong and yields uncertainties of greater than a factor of 2 in the estimated high-pressure rate coefficient. Here, the transition from long-range to short-range behavior was presumed to occur at a C⋯Cl separation of 4.0 Å. This separation roughly corresponds to the location at which the bonding interactions begin to exceed the long-range interactions and the various electronic states begin to diverge. Furthermore, as demonstrated below, this value also allowed for accurate modeling of the present experimental data. However, variation of this location by just ±0.2 Å yielded variations of nearly a factor of 2 in the predicted high-pressure rate coefficient. Thus, the present theoretical results cannot by themselves be taken to provide a reliable prediction for the high-pressure rate coefficient.
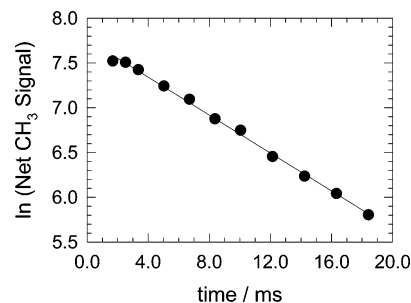
Figure 1. First-order decay plot of the natural logarithm of the net CH_3 signal vs time at $T = 298$ K and $P = 1.00$ Torr. $[CH_3]_0 = 2.92 \times 10^{11}$ molecules cm^{-3}, $[Cl]_{mean} = 6.21 \times 10^{12}$ atoms cm^{-3}, $[CH_4]_0 = 2.57 \times 10^{12}$ molecules cm^{-3}, $[HCl]_0 = 5.22 \times 10^{14}$ molecules cm^{-3}, $k_{corr} = 38.77$ s^{-1}.

The temperature- and pressure-dependent rate coefficients for the Cl + CH_3 association reaction were computed from a two-dimensional solution to the master equation[37,38] involving multistep vibrational energy transfers for the excited intermediate (CH_3Cl^*). A more detailed description of this two-dimensional solution was provided in our recent study of CH_4 dissociation.[39] The Variflex code[40] was used in these evaluations, with the solution being obtained from an inversion-based approach. An energy grain size of 20 cm^{-1} and an angular momentum grain size of 2 au allowed for convergence in the energy and angular-momentum integrations. This grain size provided converged results for the range of temperatures studied with the energy spanning the range from −2000 to 2400 cm^{-1} above the asymptote. The total angular momentum, J, covered the range from 0 to 140 in steps of 2 for the E-/J-resolved calculation.

A parametrized exponential down model[37] of energy transfer from CH_3Cl^* to He was assumed because there is no suitable a priori means for obtaining quantitative estimates for the energy-transfer function. A Lennard-Jones model for the He/CH_3Cl collision frequency was initially employed with σ and ϵ values[41] of 3.36 Å and 62 K, respectively. However, with these values, the low-pressure rate tended to be too low, even for quite large values of the average energy transferred in a single collision. Various trajectory studies have suggested that the Lennard-Jones model somewhat underestimates the collision frequency.[42,43] Thus, in the final analysis, we simply employed a collision frequency given by 1.3 times that obtained from the Lennard-Jones model. With this increase, we found, as illustrated below, that an α_{down} value of 400 cm^{-1} yielded rate coefficients in best agreement with the experimental data. This value of α_{down} corresponds to a $\langle \Delta E_{down} \rangle$ value of 387 cm^{-1} and $\langle \Delta E_{tot} \rangle$ values of −248, −264, and −282 cm^{-1} at $T = 298$, 250, and 202 K, respectively. Notably, the data could have been equally well modeled by increasing the density of states for CH_3Cl at the dissociation threshold by about a factor of 2, to account for possible anharmonicity corrections. Because of the small number of vibrational modes and their high frequencies, increasing the dissociation energy has only a modest effect on this state density.

The structures, vibrational energies, and rotational constants of CH_3 and CH_3Cl, for use in calculating partition functions, were taken from experimental studies.[44−47] The electronic degeneracies and a splitting of the Cl-atom $^2P_{1/2}-^2P_{3/2}$ levels of 882.35 cm^{-1} were also used.[48]

Results

Figure 1 shows a typical temporal profile of the CH_3 signal measured at $m/z = 15$ with $[Cl]_{mean} = 6.21 \times 10^{12}$ atoms cm^{-3}, $T = 298$ K, and $P = 1$ Torr. The reaction time was derived

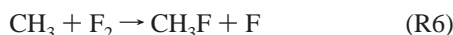**TABLE 1: Calculated Rate Coefficients for the CH$_3$ + CH$_3$ Reaction**

T/K	P/Torr	$k_7/10^{-11}$ cm^3 molecule^{-1} s^{-1}
202	0.300	4.88
202	0.500	5.38
202	1.00	5.83
202	1.50	6.00
202	2.00	6.09
250	0.300	2.89
250	0.500	3.50
250	1.00	4.27
250	1.50	4.67
250	2.00	4.91
298	0.300	1.78
298	0.500	2.25
298	1.00	2.97
298	1.50	3.40
298	2.00	3.70

from the measured distance between the tip of the movable injector and the pinhole and the linear velocity of the gas, calculated from the measured pressure and gas flow rates. The decay of CH$_3$ was pseudo-first-order in all cases and can be represented by

$$\ln [CH_3] = -k_{obs}t + \ln [CH_3]_0 \qquad (7)$$

However, secondary chemistry effects were not negligible, so the decays of CH$_3$ were corrected for these and for the effects of both axial and radial diffusion. The data analysis for the set of experiments at each temperature and pressure was a four-step process. The corrections for secondary chemistry and for axial and radial diffusion were done in separate steps, because the computer fitting programs used could not fit the data for both secondary chemistry and diffusion effects simultaneously.

The set of experiments for each temperature and pressure was corrected first for secondary chemistry by a one-parameter fitting of each CH$_3$ decay curve to a numerical simulation of the reaction system using the Facsimile program.[49] The reaction mechanism used in the numerical simulation was the following

$$F + HCl \rightarrow Cl + HF \qquad (R3)$$

$$F + CH_4 \rightarrow CH_3 + HF \qquad (R4)$$

$$CH_3 + Cl + M \rightarrow CH_3Cl + M \qquad (R2)$$

$$Cl + CH_4 \rightarrow HCl + CH_3 \qquad (R1)$$

$$CH_3 + F_2 \rightarrow CH_3F + F \qquad (R6)$$

$$CH_3 + CH_3 + M \rightarrow C_2H_6 + M \qquad (R7)$$

The temperature-dependent rate coefficients for reaction R1, where chlorine atoms react with residual methane, were calculated from the expression[50]

$$k_1(200-300 \text{ K}) = 9.6 \times 10^{-12} \text{ (cm}^3 \text{ molecule}^{-1} \text{ s}^{-1})$$
$$\exp(-1360 \text{ K}/T)$$

The expressions for the temperature-dependent rate coefficient for reactions R3 and R4 are shown in the Experimental Section. The rate coefficients used for the reaction of methyl radicals with residual molecular fluorine (R6) from the microwave discharge were calculated from the expression[16]

$$k_6(139-294 \text{ K}) = 7.0 \times 10^{-12} \text{ (cm}^3 \text{ molecule}^{-1} \text{ s}^{-1})$$
$$\exp(-490 \text{ K}/T)$$

The methyl radical self-recombination reaction (R7) is both temperature- and pressure-dependent under the physical conditions of this study. Because experimentally measured rate coefficients are not available for all of these physical conditions, the rate coefficients for reaction R7 were calculated using eqs 12 and 14 from ref 15a, which are shown below. The calculated rate coefficients are listed in Table 1.

$$k = \frac{-(k_\infty + k_0 M) + \sqrt{(k_\infty + k_0 M)^2 + 4(J_{5/2} - 1)k_\infty k_0 M}}{2(J_{5/2} - 1)}$$

$$k_0 = 5.822 \times 10^{-28} \exp(564.54/T)$$

$$k_\infty = 4.504 \times 10^{-11} \exp(70.12/T)$$

The pseudo-first-order rate coefficients (k_{first}) derived from the numerical simulations are corrected for secondary chemistry except for loss of CH$_3$ at the wall of the flow tube and possibly by reaction of CH$_3$ with excess HCl, the concentration of which was relatively constant for all experiments. These two loss processes can be represented by the first-order rate coefficient k_w. The second step of our data analysis determined k_w, which was needed in the correction for the diffusion effects. The correction for axial diffusion of the methyl radical along the flow tube was relatively simple with an analytical equation, whereas the correction for radial diffusion of the methyl radical to the wall of the flow tube was complex and required a numerical solution. For the determination of k_w, the pseudo-first-order rate coefficients, k_{first}, for the set of experiments at each temperature and pressure combination were corrected for axial diffusion by the equation:

$$k'_{corr} = k_{first}[1 + (D_{CH3}k_{first}/v^2)] \qquad (8)$$

In eq 8, D_{CH3} is the diffusion coefficient of CH$_3$ in He, and v is the linear velocity of the gas in the flow tube. D_{CH3} was estimated to be 905 cm^2 s^{-1} at $T = 298$ K and $P = 1$ Torr using the method of Lewis et al.[51] A $T^{3/2}$ dependence was assumed to estimate D_{CH3} at $T = 250$ and 202 K, and a $1/P$ dependence was assumed for pressure. The axial diffusion correction was less than 6% of the observed pseudo-first-order rate coefficient for $P = 0.3$ Torr and less than 3% in all other cases.

The partially corrected pseudo-first-order rate coefficient is given by

$$k'_{corr} = k'_2[Cl] + k_w \qquad (9)$$

where k'_2 is a second-order rate coefficient for R2 that has been corrected for secondary chemistry and axial diffusion but not radial diffusion. The intercepts of graphs of k'_{corr} versus [Cl]$_{mean}$ directly yielded k_w.

The third step of the data analysis corrected k_{first} for both axial and radial diffusion. The pseudo-first-order rate coefficient, k_{first}, has been corrected only for secondary chemistry. Reference 52 presents a numerical method and a Fortran program to correct first-order rate coefficients for both axial diffusion and radial diffusion. The input parameters from our experiments to the Fortran program were k_{first}, k_w, D_{CH3}, and an initial value for the corrected first-order rate coefficient, which was $1.2k_{first}$; these input parameters were in the required dimensionless format and
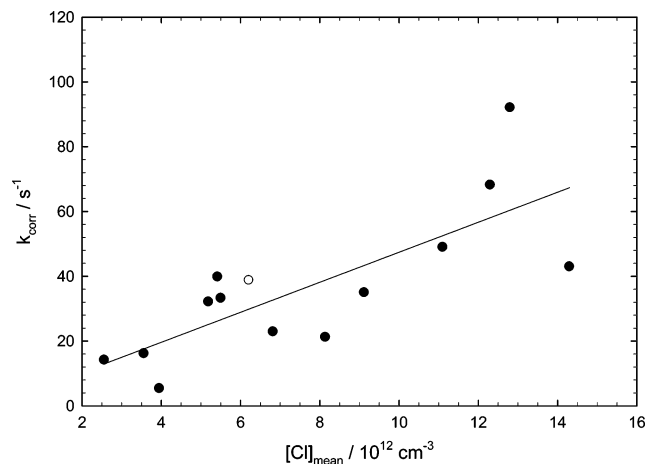
Figure 2. Plot of k_{corr} vs $[Cl]_{mean}$ at $T = 298$ K and $P = 1.00$ Torr. The open circle represents the data of Figure 1. The line is a linear least-squares fit to the data and yields a k_2 value of 4.63×10^{-12} cm^3 molecule^{-1} s^{-1}.

TABLE 2: Measured Rate Coefficients for the Cl + CH$_3$ Reaction

P/ Torr	T/ K	no. of expts	range of $[Cl]_{mean}$/ 10^{12} atoms cm^{-3}	range of $[Cl]_0/[CH_3]_0$	$k_2/10^{-12}$ cm^3 molecule^{-1} s^{-1}
0.30	202	9	3.59−16.3	20.4−46.1	8.36 ± 2.07
0.50	202	6	2.89−9.43	21.8−59.6	13.3 ± 1.9
1.00	202	5	3.31−9.97	18.3−46.5	16.3 ± 3.0
1.50	202	7	3.32−14.5	23.9−66.9	16.8 ± 2.7
2.00	202	6	3.52−8.89	23.4−47.9	17.7 ± 5.7
0.30	250	8	2.94−12.9	11.4−33.0	4.76 ± 1.23
0.50	250	5	2.19−8.97	17.6−50.0	8.12 ± 2.42
1.00	250	5	2.42−9.90	14.0−49.1	9.51 ± 1.34
1.50	250	6	2.26−10.8	12.1−49.4	13.2 ± 2.7
2.00	250	5	2.95−11.3	12.7−38.0	10.7 ± 1.9
0.30	298	6	2.31−11.2	9.4−26.8	0.744 ± 0.445
0.50	298	6	3.79−14.2	21.2−56.9	2.91 ± 1.34
1.00	298	14	2.56−14.3	12.1−36.6	4.63 ± 1.24
1.50	298	5	2.87−10.6	15.7−35.1	5.71 ± 1.15
2.00	298	8	3.15−16.5	15.7−51.2	5.27 ± 1.55

were within the range of parameter values which had been tested for convergence in the solutions.[52] The output pseudo-first-order rate coefficients, k_{corr}, were, at that point, corrected for secondary chemistry and for both axial diffusion and radial diffusion. The correction for radial diffusion was less than 2.5% except at the two highest pressures at $T = 202$ K, where this correction was less than 3% for $P = 1.5$ Torr and less than 4% for $P = 2$ Torr.

These rate coefficients could be represented by the equation

$$k_{corr} = k_2[Cl]_{mean} \tag{10}$$

where k_2 is the second-order rate coefficient for R2.

In the fourth and final step of the data analysis, the slope of the graph of k_{corr} versus $[Cl]_{mean}$ yielded the bimolecular rate coefficient k_2 for the reaction of CH$_3$ + Cl for a given temperature and pressure. In all cases, the intercept differed from 0 by less than 1.5 s^{-1}. Figure 2 shows a plot of k_{corr} vs $[Cl]_{mean}$ for $T = 298$ K and $P = 1$ Torr. The solid line is a linear least-squares fit to the data.

Table 2 summarizes the rate coefficient measurements. The details for each experiment are included in the Supporting Information in Tables S1−S3. The experimental uncertainties in the rate coefficients are given in parentheses. The uncertainties were estimated by adding in quadrature the independent experimental errors (assumed to be 10% for the concentration
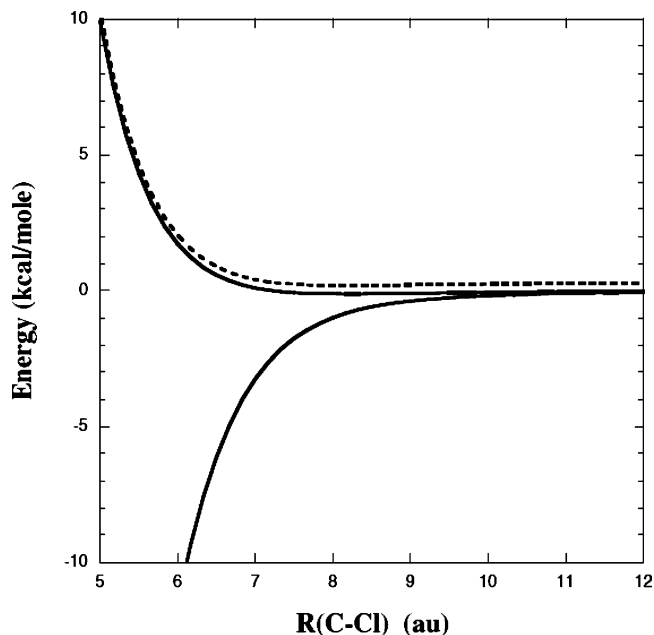

Figure 3. Plot of the minimum-energy-path potentials for the three lowest electronic states of CH$_3$ + Cl as evaluated with CAS+1+2+QC/ aug-cc-pvtz calculations. The solid lines are the two 1A′ states, and the dashed line is the 1A″ state.
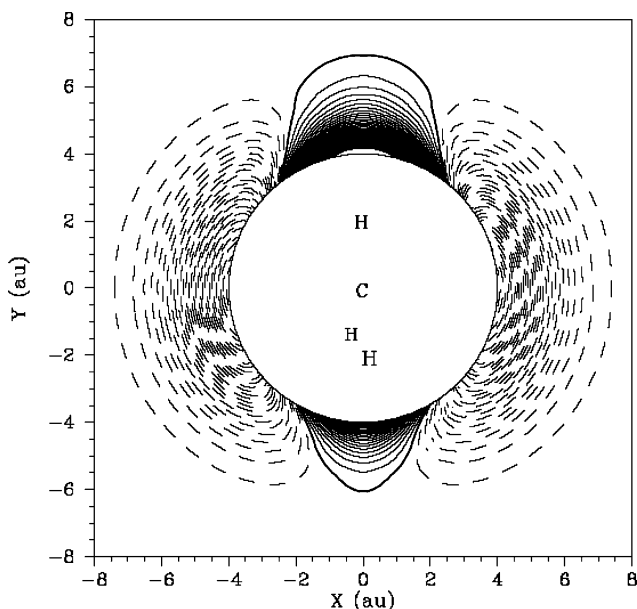
Figure 4. Two-dimensional plot of the Cl + CH$_3$ potential energy surface. The plotting plane contains the methyl C_3 axis and one CH bond. The heavy solid contour is the zero-energy contour (defined to be the energy of the separated reactants), the lighter solid contours are positive (repulsive with respect to reactants), and the dashed contours are negative (attractive). The contour increment is 2 kcal mol^{-1}, and all distances are shown in atomic units (one atomic unit = 0.52918 Å).

of Cl, 5% for the total gas flow rate, 2% for the temperature, 2% for the pressure, and 2% for the timing) and the statistical error (1σ) from the plots of k_{corr} versus $[Cl]_{mean}$.

The CAS+1+2+QC/aug-cc-pvtz-calculated interaction between CH$_3$ and Cl in C_{3v} symmetry is illustrated in Figure 3 for the three lowest electronic states. The ground electronic state is seen to diverge from the excited electronic states at $R \approx 8a_0$ = 4.2 Å. A contour plot of the interaction energies for the ground electronic state is provided in Figure 4.
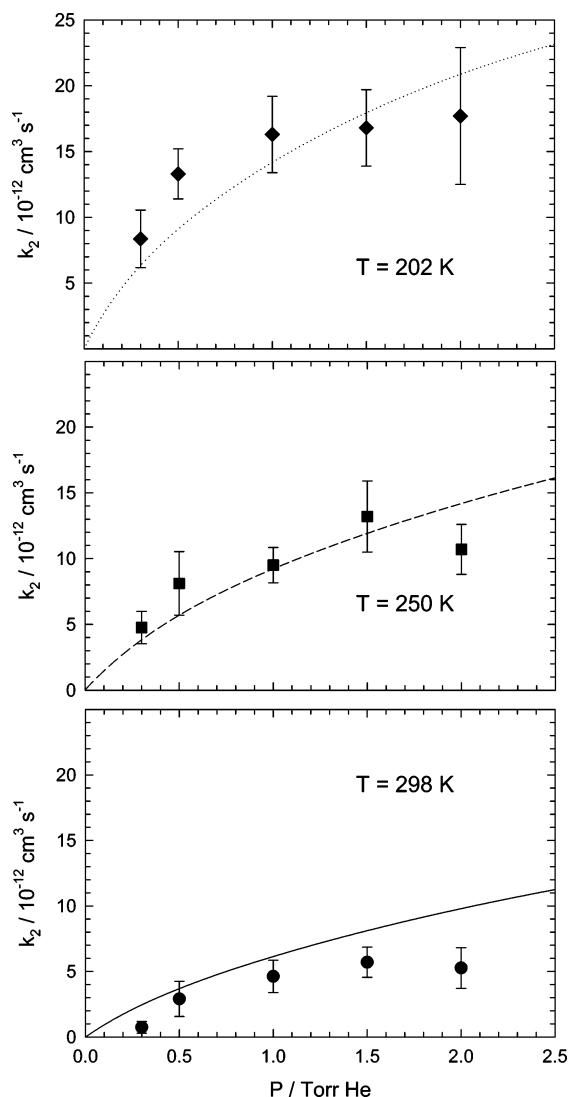
Figure 5. Plot of experimental (data points) and calculated (lines) rate coefficients of Cl + CH$_3$ as a function of He bath gas pressure at T = 202, 250, and 298 K. The pressure axis has the same scale for all three plots.

Discussion

The rate coefficients of Table 2 are plotted as a function of pressure in Figure 5. For a given temperature, the rate coefficient increases with increasing pressure, indicating that the reaction is in the falloff regime under these conditions. For a given pressure, the rate coefficient increases with decreasing temperature. This behavior of k_2 with respect to temperature suggests that the Cl + CH$_3$ reaction occurs without a significant barrier. This observation is in agreement with the potential energy diagrams of Figures 3 and 4.

The lines of Figure 5 are the theoretical predictions from the variational RRKM-based master-equation calculations. At the three temperatures studied, the RRKM-based rate coefficients either pass through the error bars or come very close to their termini. The experimental results at the lowest pressures approach the low-pressure limit. This low-pressure limit is determined by the density of states at the dissociation threshold, by the collision frequency, and by the collision efficiency. Here, we find that implementation of a collision frequency of 1.3 times the Lennard-Jones value and an α_{down} value of 400 cm^{-1} (both of which are somewhat larger than normal, but not unreasonably so) yields good agreement with the experimental observations.
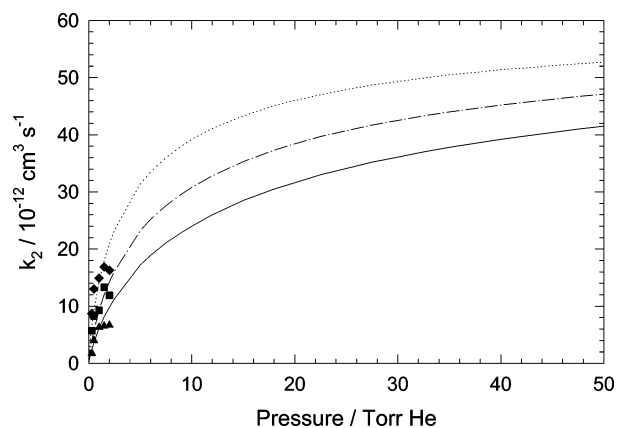

Figure 6. As in Figure 5 but with the pressure range extended to 50 Torr He. The high-pressure limiting rate coefficient from the RRKM calculations is $k_{2,\infty} = 6.0 \times 10^{-11}$ cm^3 molecule^{-1} s^{-1}, independent of temperature. At 50 Torr He, the calculated rate coefficients are greater than 70% of the value of $k_{2,\infty}$ at all three temperatures. Dotted line and solid diamond, 202 K; dashed line and solid square, 250 K; solid line and solid triangle, 298 K.

Similarly enhanced values of α_{down} have been encountered in the modeling of other chlorinated reactions.[53] Alternatively, the density of states might be somewhat increased by anharmonicities in the vibrational modes or an underestimate of the dissociation threshold.

Figure 6 shows a plot of k_2 versus the pressure of He over the pressure range 0−50 Torr. At 50 Torr He, the calculated rate coefficients are greater than 70% of the value of $k_{2,\infty}$ at all three temperatures ($k_{2,\infty} = 6.0 \times 10^{-11}$ cm^3 molecule^{-1} s^{-1} for all three temperatures). The high level of agreement between the theoretical and experimental rate coefficients over the range of pressure studied suggests that the calculated falloff curves of Figure 5 can be considered to be reasonably reliable extrapolations of the data. It is particularly difficult to reproduce the experimental data with any increase in the high-pressure-limit rate coefficient.

In a previous experimental study[13] of the photochlorination of methane, the rate coefficient of the Cl + CH$_3$ reaction at T = 298−429 K and P = 49−212 Torr CO$_2$ was extracted in an indirect manner. The high-pressure limiting rate coefficient, $k_{2,\infty}$, was found to be described by the equation 3.7×10^{-10} exp(−185/T) for T = 298−429 K. The value of $k_{2,\infty}$(298 K) = 2.0 × 10^{-10} cm^3 molecule^{-1} s^{-1} is more than a factor of 3 higher than our calculated value (Figure 6). Because of the complex, indirect way in which Timonen et al.[13] derived k_2, we believe the results of Timonen et al. are unreliable and should not be used.

A few experiments have also probed the dissociation of CH$_3$-Cl, but at higher temperatures (1200−2100 K).[54−56] Figure 7 provides a comparison of predictions from the present theoretical model with the data from these experimental studies. The theoretical predictions for a pressure of 760 Torr are based on a CH$_4$ bath gas, whereas those for the other pressures are for an Ar bath gas, in keeping with the related experimental studies. In each case, a collision frequency equal to 1.3 times the Lennard-Jones values was employed for consistency with the low-temperature model. α_{down} was treated as a fitting parameter, with the form 400[T(K)/298]$^{0.4}$ cm^{-1} providing a satisfactory reproduction of the experimental results from both refs 54 and 56. In contrast, the data from ref 55 could not be reproduced. The prediction of an increase in α_{down} with temperature is in keeping with the observations from a number of related studies;[57−61] however, the exponent has been closer to unity in
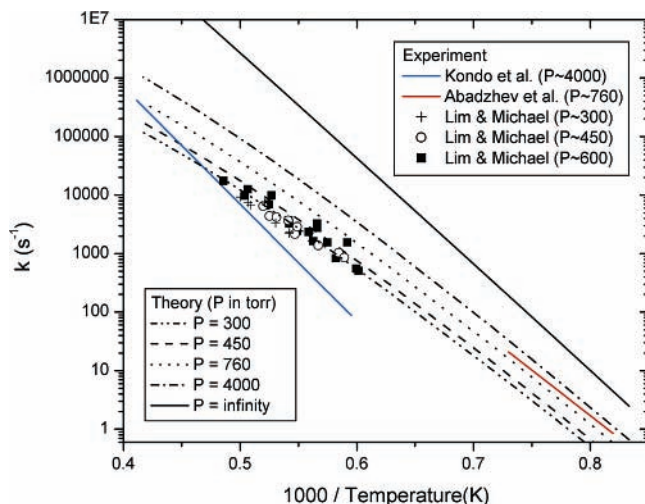
Figure 7. Plot of the temperature dependence of the CH₃Cl dissociation rate constant for a range of pressures from both theory and experiment.

our prior studies.[39,62] It is unclear whether the small magnitude of this exponent is a meaningful result or whether there is simply insufficient information to accurately determine α_{down} in either the low-temperature or the high-temperature limit.

The present predictions for the CH₃ + Cl association rate coefficients over the 200−2000 K temperature range and the $(1.0 \times 10^{-2})-(1.0 \times 10^{5})$ Torr pressure range were fit to the Troe form.[63] The high-pressure limit was reproduced to within 2% by the modified Arrhenius expression

$$k_{\infty}(T) = 5.09 \times 10^{-11} \, (T/298)^{0.300}$$
$$\exp(54.6/T) \, \text{cm}^3 \, \text{molecule}^{-1} \, \text{s}^{-1}$$

where T was in Kelvin for each case. The low-pressure limit was reproduced to within about 15% by the modified Arrhenius expression

$$k_0(T) = 6.27 \times 10^{-27} \, (T/298)^{-4.67}$$
$$\exp(-846/T) \, \text{cm}^6 \, \text{molecule}^{-2} \, \text{s}^{-1}$$

The pressure dependence was reproduced to within about 20% by the modified Arrhenius form

$$F_{cent}(T) = 0.674(T/298)^{-0.414} \exp(-38.7/T)$$

for the central broadening factor.

An experimental determination[8] of the rate coefficient for the reaction Cl + CH₄ → HCl + CH₃ was carried out to test the discharge-flow resonance fluorescence technique for possible effects of secondary chemistry (i.e., Cl + CH₃ + M → ClCH₃ + M) below $T = 300$ K, where disagreement among previous studies on the value of k_1 is greatest. Wang and Keyser[8] concluded that Cl + CH₃ was most likely interfering in their measurements of the rate coefficient of Cl + CH₄ and further stated that k_2(298 K, 1 Torr He) must be greater than or equal to 5×10^{-11} cm³ molecule⁻¹ s⁻¹ to interfere in measurements of k_1. We measured k_2(298 K, 1 Torr He) = 4.5×10^{-12} cm³ molecule⁻¹ s⁻¹. Therefore, Cl + CH₃ + M cannot be interfering in the laboratory measurements of the Cl + CH₄ rate coefficient; some other explanation must be sought to reconcile the disparate low-temperature rate coefficient data for R1.

A suggestion was made recently in the literature that resonance fluorescence detection of Cl might be a deficient experimental method for measuring k_1.[64] Michelson and Sim-

pson[64] stated that CH₄ promoted to the 3s Rydberg state (by absorption of Cl resonance radiation near $\lambda = 139$ nm) is much more likely to dissociate than to relax to a lower electronic state, yielding CH₃, CH₂, H, and H₂. They concluded that reaction of Cl with these fragments would yield rate coefficients of R1 that were too large and that studies using alternative detection techniques should be carried out for a proper evaluation of k_1.

However, a reasonable estimate of the CH₃ concentration formed via photolysis of CH₄ by vacuum-UV radiation from a typical Cl resonance lamp (not a Cl photolysis lamp) is [CH₃] $\leq 3 \times 10^{10}$ molecule cm⁻³. This is 5 orders of magnitude less than the typical CH₄ concentration employed in either photolysis or flow-tube studies. The ratio of the low-temperature rate coefficients for the two reactions is $k(\text{Cl} + \text{CH}_4)/k(\text{Cl} + \text{CH}_3)$ $\approx 10^{-3}$. Thus, the contribution of Cl + CH₃ (where CH₃ is formed via photolysis of CH₄ by a Cl resonance lamp) to the loss of Cl via Cl + CH₄ is on the order of 1% and entirely negligible.

Finally, we assess the results of an experimental study of the measurement of rate coefficients[65] for the related reaction CH₃ + Br + He → CH₃Br + He at $T = 297$ K over the pressure range of 1−100 bar helium. Using the relative-rate method (relative to CH₃ + CH₃) and the laser photolysis−transient UV spectroscopy technique, the authors found that the rate coefficient is in the falloff regime over this very large and very high pressure range. They found that the high-pressure limiting rate coefficient is 1.19×10^{-10} cm³ molecule⁻¹ s⁻¹ at $T = 297$ K. The observation of a pressure dependence above 1 bar for this analogous reaction is very different from our theoretical results (and not consistent with our experimental results) for CH₃ + Cl. From our theoretical results, k_2(298 K) is 70% of the value of $k_{2,\infty}$ at 50 Torr and $k_2 = 0.99k_{2,\infty}$ at 1 bar. The large difference in the pressure dependence of the rate coefficient for these two reactions is difficult to reconcile. The very large pressures required to stabilize the CH₃Br* adduct imply that this species is formed with much more internal energy than CH₃-Cl*. For this to be true, the potential energy surface for CH₃ + Br and/or the location of the transition state on the reaction coordinate would have to be very different from those for CH₃ + Cl reaction. We recommend additional experimental and theoretical studies for CH₃ + Br + M → CH₃Br + M.

Supporting Information Available: For each experiment, the concentration of each reactant and the corrected first-order

rate coefficient, k_{corr}, are contained in Tables S1−S3. Table S1 has the data at each pressure for $T = 202$ K, Table S2 for $T = 250$ K, and Table S3 for $T = 298$ K. For each pressure, k_w derived from the second step of the data analysis is included. This material is available free of charge via the Internet at http://pubs.acs.org.

References and Notes

(1) Finlayson-Pitts, B. J.; Pitts, J. N., Jr. *Atmospheric Chemistry: Fundamentals and Experimental Techniques*; John Wiley & Sons: New York, 1986.

(2) Wayne, R. P. *Chemistry of Atmospheres*; Clarendon Press: Oxford, U.K., 1991.

(3) Molina, M. J.; Rowland, F. S. *Nature* **1974**, *249*, 810.

(4) DeMore, W. B. *J. Geophys. Res.* **1991**, *96*, 4995.

(5) Lin, C. L.; Leu, M. T.; DeMore, W. B. *J. Phys. Chem.* **1978**, *82*, 1772.

(6) Keyser, L. F. *J. Chem. Phys.* **1978**, *69*, 214.

(7) Zahniser, M. S.; Berquist, B. M.; Kaufman, F. *Int. J. Chem. Kinet.* **1978**, *10*, 15.

(8) Wang, J. J.; Keyser, L. F. *J. Phys. Chem. A* **1999**, *103*, 7460.

(9) Watson, R.; Machado, G.; Fischer, S.; Davis, D. D. *J. Chem. Phys.* **1976**, *65*, 2126.

(10) Manning, R. G.; Kurylo, M. J. *J. Phys. Chem.* **1977**, *81*, 291.

(11) Whytock, D. A.; Lee, J. H.; Michael, J. V.; Payne, W. A.; Stief, L. J. *J. Phys. Chem.* **1977**, *66*, 2690.

(12) Michelsen, H. A.; Salawitch, R. J.; Gunson, M. R.; Aellig, C.; Kämpfer, N.; Abbas, M. M.; Abrams, M. C.; Brown, T. L.; Chang, A. Y.; Goldman, A.; Irion, F. W.; Newchurch, M. J.; Rinsland, C. P.; Stiller, G. P.; Zander, R. *Geophys. Res. Lett.* **1996**, *23*, 2361.

(13) Timonen, R.; Kalliorinne, K.; Koskikallio, J. *Acta Chem. Scand. A* **1986**, *40*, 459.

(14) Brunning, J.; Stief, L. J. *J. Chem. Phys.* **1986**, *84*, 4371.

(15) (a) Cody, R. J.; Romani, P. N.; Nesbitt, F. L.; Iannone, M. A.; Tardy, D. C.; Stief, L. J. *J. Geophys. Res.* **2003**, *108* (E11), article no. 5119. (b) Pimentel, A. S.; Payne, W. A.; Nesbitt, F. L.; Cody, R. J.; Stief, L. J. *J. Phys. Chem. A* **2004**, *108*, 7204. (c) Mitchell, M. B.; Brunning, J.; Payne, W. A.; Stief, L. J. *J. Phys. Chem.* **1988**, *92*, 1502. (d) Cody, R. J.; Payne, W. A.; Thorn, R. P.; Nesbitt, F. L.; Iannone, M. A.; Tardy, D. C.; Stief, L. J. *J. Phys. Chem. A* **2002**, *106*, 6060.

(16) . Moore, C. M.; Smith, I. W. M.; Stewart, D. W. A. *Int. J. Chem. Kinet.* **1994**, *26*, 813.

(17) Atkinson, R.; Baulch, D. L.; Cox, R. A.; Crowley, J. N.; Hampson, R. F, Jr.; Hynes, R. G.; Jenkin, M. E.; Kerr, J. A.; Rossi, M. J.; Troe, J. *Summary of Evaluated Kinetic and Photochemical Data for Atmospheric Chemistry*; IUPAC Subcommittee on Gas Kinetic Data Evaluation for Atmospheric Chemistry: University of Cambridge, U.K., March, 2005 (Web Version); available at http://www.iupac-kinetic.ch.cam.ac.uk/summary/IUPACsumm_web_March2005.pdf; accessed October, 2005.

(18) Nesbitt, F. L.; Cody, R. J.; Dalton, D. A.; Riffault, V.; Bedjanian, Y.; Le Bras, G. *J. Phys. Chem. A* **2004**, *108*, 1726.

(19) Werner, H.-J.; Knowles, P. J. *J. Chem. Phys.* **1985**, *82*, 5053.

(20) Knowles, P. J.; Werner, H.-J. *Chem. Phys. Lett.* **1985**, *115*, 249.

(21) Werner, H.-J.; Knowles, P. J. *J. Chem. Phys.* **1988**, *89*, 5803.

(22) Knowles, P. J.; Werner, H.-J. *Chem. Phys. Lett.* **1988**, *145*, 514.

(23) Kendall, R.A.; Dunning, T. H., Jr.; Harrison, R. J. *J. Chem. Phys.* **1992**, *96*, 6796.

(24) Woon, D. E.; Dunning, T. H., Jr. *J. Chem. Phys.* **1993**, *98*, 1358.

(25) Knowles, P. J.; Hampel, C.; Werner, H.-J. *J. Chem. Phys.* **1993**, *99*, 5219; *J. Chem. Phys.* **2000**, *112*, 3106.

(26) Dunning, T. H. *J. Chem. Phys.* **1989**, *90*, 1007.

(27) Martin, J. M. L. *Chem. Phys. Lett.* **1996**, *269*, 669.

(28) Feller, D.; Dixon, D. A. *J. Chem. Phys.* **2001**, *115*, 3484.

(29) Becke, A. D. *J. Chem. Phys.* **1993**, *98*, 5648.

(30) Hehre, W. J.; Radom, L.; Pople, J. A.; Schleyer, P. v. R. *Ab Initio Molecular Orbital Theory*; Wiley: New York, 1987.

(31) Amos, R. D.; Bernhardsson, A.; Berning, A.; Celani, P.; Cooper, D. L.; Deegan, M. J. O.; Dobbyn, A. J.; Eckert, F.; Hampel, C.; Hetzer, G.; Knowles, P. J.; Korona, T.; Lindh, R.; Lloyd, A. W.; McNicholas, S. J.; Manby, F. R.; Meyer, W.; Mura, M. E.; Nicklass, A.; Palmieri, P.; Pitzer, R.; Rauhut, G.; Schutz, M.; Schumann, U.; Stoll, H.; Stone, A. J.; Tarroni, R.; Thorsteinsson, T.; Werner, H.-J. *MOLPRO, a package of ab initio programs designed by H.-J. Werner and P. J. Knowles*, version 2002.1.

(32) Frisch, M. J.; Trucks, G. W.; Schlegel, H. B.; Scuseria, G. E.; Robb, M. A.; Cheeseman, J. R.; Zakrzewski, V. G.; Montgomery, J. A., Jr.;Stratmann, R. E.; Burant, J. C.; Dapprich, S.; Millam, J. M.; Daniels, A. D.; Kudin, K. N.; Strain, M. C.; Farkas, O.; Tomasi, J.; Barone, V.; Cossi, M.; Cammi, R.; Mennucci, B.; Pomelli, C.; Adamo, C.; Clifford, S.; Ochterski, J.; Petersson, G. A.; Ayala, P. Y.; Cui, Q.; Morokuma, K.; Malick, D. K.; Rabuck, A. D.; Raghavachari, K.; Foresman, J. B.; Cioslowski, J.; Ortiz, J. V.; Stefanov, B. B.; Liu, G.; Liashenko, A.; Piskorz, P.; Komaromi, I.; Gomperts, R.; Martin, R. L.; Fox, D. J.; Keith, T.; Al-Laham, M. A.; Peng, C. Y.; Nanayakkara, A.; Gonzalez, C.; Challacombe, M.; Gill, P. M. W.; Johnson, B.; Chen, W.; Wong, M. W.; Andres, J. L.; Head-Gordon, M.; Replogle, E. S.; Pople, J. A. *Gaussian 98*; Revision A.7; Gaussian, Inc.: Pittsburgh, PA, 1998.

(33) Klippenstein, S. J. *J. Chem. Phys.* **1991**, *94*, 6469. Klippenstein, S. J. *J. Chem. Phys.* **1992**, *96*, 367. Klippenstein, S. J. *J. Phys. Chem.* **1994**, *98*, 11459.

(34) Tashiro, M.; Schinke, R. *J. Chem. Phys.* **2003**, *119*, 10186.

(35) Klippenstein, S. J.; Khundkar, L. R.; Zewail, A. H.; Marcus, R. A. *J. Chem. Phys.* **1988**, *89*, 4761.

(36) Harding, L. B.; Klippenstein, S. J.; Georgievskii, Y. *Proc. Comb. Symp. Inst.* **2005**, *30*, 945.

(37) Gilbert, R. G.; Smith, S. C. *Theory of Unimolecular and Recombination Reactions*; Blackwell Scientific: Carlton, Australia, 1990.

(38) Holbrook, K. A.; Pilling, M. J.; Robertson, S. H. *Unimolecular Reactions*; Wiley: New York, 1996.

(39) Miller, J. A.; Klippenstein, S. J.; Raffy, C. *J. Phys. Chem. A* **2002**, *106*, 4904.

(40) Klippenstein, S. J.; Wagner, A. F.; Dunbar, R. C.; Wardlaw, D. M.; Robertson, S. H. *VARIFLEX*, version 1.00; Argonne National Laboratory, Argonne, IL, 1999.

(41) Hirschfelder, J. O.; Curtiss, C. F.; Bird, R. B. *Molecular Theory of Gases and Liquids*; John Wiley & Sons, Inc.: New York, 1954.

(42) Brown, N. J; Miller, J. A. *J. Chem. Phys.* **1984**, *80*, 5568.

(43) Nordholm, S.; Schranz, H. W. In *Vibrational Energy Transfer in Large and Small Molecules*; Barker, J. A., Ed.; JAI Press: Greenwich, CT, 1995; Vol. 2A, pp 245−281.

(44) Jacox, M. E. *J. Phys. Chem.Ref. Data* **1994**, Monograph 3.

(45) Yamada, C.; Hirota, E.; Kawaguchi, K. *J. Chem. Phys.* **1981**, *75*, 5256.

(46) Dickson, A. D.; Mills, I. M.; Crawford, B. *J. Chem. Phys.* **1957**, *27*, 445.

(47) Herzberg, G. *Electronic Spectra and Electronic Structure of Polyatomic Molecules*; Van Nostrand: New York, 1966

(48) *NIST Atomic Spectra Database*; National Institute of Standards and Technology (NIST): Gaithersburg, MD, 2006; available at http://physics.nist.gov/cgi-bin/AtData/main_asd, accessed June, 2004.

(49) Curtis, A. R.; Sweetenhan, W. P. *Facsimile Program*; Report R-12805; U.K. Atomic Energy Research Establishment: Harwell, U.K., 1987.

(50) Sander, S. P.; Friedl, R. R.; Golden, D. M.; Kurylo, M. J.; Huie, R. E.; Orkin, V. L.; Moortgat, G. K.; Ravishankara, A. R.; Kolb, C. E.; Molina, M. J.; Finlayson-Pitts, B. J. *Chemical Kinetics and Photochemical Data for Use in Atmospheric Studies: Evaluation Number 14*; JPL Publication 02-25; NASA Panel for Data Evaluation, Jet Propulsion Laboratory, California Institute of Technology: Pasadena, CA, 2003.

(51) Lewis, R. S.; Sander, S. A.; Wagner, W.; Watson, R. T. *J. Phys. Chem.* **1996**, *100*, 13594.

(52) Brown, R. L. *J. Res. Natl. Bur. Stand.* **1978**, *83*, 1.

(53) Kumaran, S. S.; Su, M. C.; Lim, K. P.; Michael, J. V.; Wagner, A. F.; Harding, L. B.; Dixon, D. A. *J. Phys. Chem.* **1996**, *100*, 7541.

(54) Lim, K. P.; Michael, J. V. *J. Chem. Phys.* **1993**, *98*, 3919.

(55) Kondo, O.; Saito, K.; Murakami, I. *Bull. Chem. Soc. Jpn.* **1980**, *53*, 2133.

(56) Abadzhev, S. S.; Dzikh, I. P.; Shevchuk, V. U. *Kinet. Catal.* **1989**, *30*, 893.

(57) Hanning-Lee, M. A.; Green, N. J. B.; Pilling, M. J.; Robertson, S. H. *J. Phys. Chem.* **1993**, *97*, 860.

(58) Feng, Y.; Nuranen, J. T.; Benesuar, A.; Knyazev, V. D.; Gutman, D.; Tsang, W. *J. Phys. Chem.* **1993**, *97*, 871.

(59) Knyazev, V. D.; Dubinsky, I. A.; Slagle, I. R.; Gutman, D. *J. Phys. Chem.* **1994**, *98*, 5279.

(60) Knyazev, V. D.; Slagle, I. R. *J. Phys. Chem.* **1996**, *100*, 16899.

(61) Knyazev, V. D.; Tsang, W. *J. Phys. Chem. A* **2000**, *104*, 10747.

(62) Miller, J. A.; Klippenstein, S. J. *J. Phys. Chem. A* **2003**, *107*, 2680.

(63) Troe, J. *J. Phys. Chem.* **1979**, *83*, 114.

(64) Michelsen, H. A.; Simpson, W. R. *J. Phys. Chem. A* **2001**, *105*, 1476.

(65) Krasnoperov, L. N.; Mehta, K. *J. Phys. Chem. A* **1999**, *103*, 8008.